Mathematical Analysis and its Contemporary Applications
Volume 6, Issue 1, 2024, 69–93
doi: 10.30495/maca.2024.2017221.1092
ISSN 2716-9898

Optimizing airfoil efficiency for offshore turbines through aerodynamic geometry enhancement

Hossein Seifi Davari*, Harun Chowdhury, Mohsen Seify Davari, and Hasan Hosseinzadeh

Abstract. Initially, the optimal Thickness-to-Camber ratio (t/c) of the SG6043 airfoil was examined across Reynolds numbers (Re) ranging from 10,000 to 500,000, typical for Small Wind Turbines (SWTs) using QBLADE software. The ideal t/c increased between 0.5 and 1.50, surpassing the SG6043 airfoil in peak Lift-to-Drag ratio coefficient (CL/CD). Subsequently, three modified airfoils were developed within the t/c range of 0.5 to 1.5. Results demonstrated improved aerodynamic coefficients in the modified airfoils as Re increased. Notably, Case 3 airfoil exhibited the highest maximum CL/CD of 176.97 at Re 500,000. Furthermore, Case 1 and Case 2 yielded maximum CL/CD values of 172.43 and 171.08, respectively. The airfoils in Cases 2, 1, and 3 achieved peak Lift Coefficients (CL) of 1.847, 1.82, and 1.77, respectively. Specifically, at Re except for 100,000, Case 2 airfoil outperformed the other modified and SG6043 airfoils in terms of CL. At $Re \leq 100,000$, the Case 1 airfoil demonstrated a higher maximum CL/CD compared to other modified and SG6043 airfoils. Across the Re range of 10,000 to 500,000, the Case 2 airfoil consistently achieved the highest peak CL/CD. This research was validated through experimental work and compared with the EYO-Series airfoils.

2020 *Mathematics Subject Classification.* 76G25.

Key words and phrases. Airfoil, Low Reynolds Numbers, Aerodynamic, QBLADE, Optimization

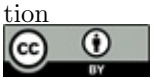

*Corresponding author.

1. Introduction

Improving the shape of airfoils enhances the effectiveness of Wind Turbines (WTs). Researchers have focused on refining WT blade airfoil shapes to boost efficiency and drive down the cost of electricity [17]. Various optimization techniques have been employed to refine these airfoil shapes [21]. In the study conducted by Martel et al. [11], the base airfoil underwent parameterization using Class Shape Transformation (CST) to introduce shape modifications. The optimization process utilized a multi-objective Non-Dominated Sorting Genetic Algorithm (GA) through MATLAB software. Their findings indicated that at an Angle of Attack (AoA) of 8°, the maximum possible CL/CD improved by up to 65.3%. Additionally, Kumawat and Ghosh [9] investigated the performance of both a thick airfoil, NACA0012, and a thin airfoil, NACA0003, at low Re. Their results demonstrated that employing camber morphing instead of a hinged flap delayed flow separation in the NACA0012 airfoil. Körpe et al. [8] analyzed the implementation of Genetic Algorithms (GA) and sequential quadratic programming for optimizing NACA 4-digit airfoils. Their findings demonstrated that employing the objective function method increased the airfoil's aerodynamic efficiency by 20%. Exploring unconventional airfoil shapes with angular leading edges for a potential rotor, Koning et al. [7] discovered a maximum increase in CL/CD by 17%. Additionally, Quan et al. [15] combined Computational Fluid Dynamics (CFD) with GA to investigate a method for optimizing form. Their objective aimed to aid researchers in developing Wind Turbine (WT) designs that operate more efficiently under local conditions. Exploring an innovative intelligence algorithm based on B-spline-defined airfoils for Low Wind Velocity (LWV) scenarios, researchers investigated its performance at Re. Their findings revealed that the B-spline method showcased superior aerodynamic characteristics under both free and fixed transitions compared to the original DU airfoils [14]. Furthermore, Deng et al. [4] delved into an inventive shape parameterization technique for airfoils. Employing the thin airfoil theory, they utilized a Fourier series to express the vortex distribution along the chord line, establishing the mean camber line of an airfoil rather than directly specifying its shape. To address and mitigate the profound dynamic stall characteristics of airfoils, Raul and Leifsson [16] explored a Surrogate-Based Optimization (SBO) method to alleviate the computational load in Aerodynamic Shape Optimization (ASO). Their findings showcased that geometric modifications led to an increase in the dynamic stall Angle of Attack (AoA). Tanürün [23] demonstrated that an adaptive flap design enhances efficiency by refining the wake and amplifying the performance behind the Wind Turbine (WT) blade. Meanwhile, Hongpeng et al. [5] investigated the effects of trailing thickness and asymmetric alteration parameters. They employed three methods—applying a zigzag trailing edge, using a Slotted Airfoil (SA), and a combined approach—to reduce the Drag coefficient (CD). Their results indicated that SAs increased CL and reduced CD notably at

high AoA. Additionally, Seifi et al. [19] illustrated that by altering the geometry of the NACA0015 airfoil at Re of 100,000 and 200,000, improvements in the wind turbine's performance could be achieved, enhancing from 0.129 to 0.152 and from 0.285 to 0.307, respectively. Furthermore, another study by Seifi et al. [18] highlighted that at low Re, the NACA0015 airfoil exhibited superior aerodynamic performance compared to the NACA0018 and NACA0021 airfoils. The aim of this study is to optimize the SG6043 airfoil specifically for small wind turbines operating at Reynolds numbers below 500,000. Given the crucial role of low Reynolds numbers in enhancing the efficiency of small wind turbines, this research focuses on leveraging the airfoil's thickness to camber ratio method to further improve its aerodynamic performance. By employing advanced optimization techniques, the study endeavors to achieve superior aerodynamic efficiency compared to commonly used airfoils (SG6043, EYO7-8, EYO8-8, and EYO9-8) in this field. Through meticulous comparison and analysis against existing research findings, the goal is to develop an optimized airfoil design that outperforms other alternatives. Ultimately, the objective is to introduce an airfoil that not only showcases heightened efficiency but also has the potential to replace current models in small wind turbine applications, significantly elevating their overall effectiveness and performance

2. Methodology

2.1. Selection of the airfoils. The study evaluates a gradient-based shape optimization methodology applied to Small Wind Turbine (SWT) airfoil blades. Utilizing the QBLADE software, a 2D potential flow solver incorporating viscous effects, alongside the Blade Element Momentum Theory (BEMT), this

methodology aims to maximize the power output of SWT blades, determined through BEMT analysis. QBLADE software has been widely employed by researchers to explore and analyze airfoil aerodynamics. Its outcomes have been corroborated through experimental validation with wind tunnel data in various studies [1, 2, 22]. The SG6043 airfoil [12, 13] was chosen as the baseline due to its commendable aerodynamic efficiency at low Re. Utilizing the QBLADE software, the baseline airfoil shape underwent optimization, enabling the creation of new airfoils by adjusting thicknesses and camber settings. These newly devised airfoils were examined to determine their maximum CL/CD across Re values ranging from 10,000 to 500,000, considering various t/c configurations. The t/c range exhibiting the highest CL/CD was used to compute the geometric parameters for the modified airfoils, aiming to ascertain their optimal aerodynamic performance. Refer to Figure 1 for the algorithm employed to identify the optimized airfoil geometries analyzed using QBLADE software. Analyses were carried out for viscous airflow at Re values spanning 10,000 to 500,000, considering angles of Attack (AoA) ranging from 0° to

20°. Details regarding the performance parameters of the three newly developed innovative airfoils are presented in the subsequent section.

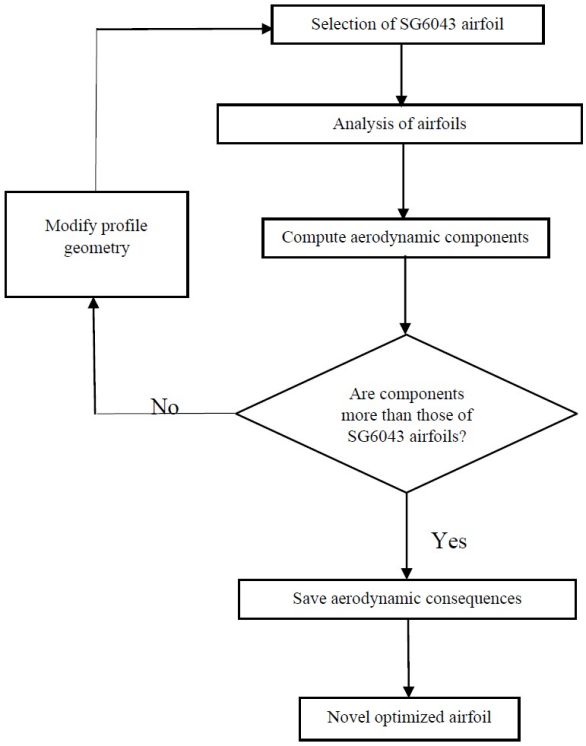

FIGURE 1. Abstract of QBLADE software process for profile experiment.

2.2. Theoretical framework. The theoretical basis for investigating with the aerodynamic characteristics of the airfoils is provided by Eqs. (1) to (3) [10]. The Reynolds number, Re, is defined by:

$$Reynolds\ number = \frac{U_{\tau e^{iC}}}{\mu} = \frac{\rho U_{\tau e^{iC}}}{\nu} \tag{1}$$

where ρ is the fluid density, μ is fluid viscosity, $\nu = \frac{\mu}{\rho}$ is the kinematic viscosity. These might be the incoming wind speed, U_{rel}, and the chord length on an airfoil. The two-dimensional lift coefficient is defined as:

$$C_l = \frac{\frac{L}{l}}{\frac{1}{2}\rho U_{\tau e^{iC}}} = \frac{\frac{\text{Lift force}}{\text{unit lenght}}}{\frac{\text{Dynamic force}}{\text{unit lenght}}} \tag{2}$$

The two-dimensional drag coefficient is defined as:

$$C_a = \frac{\frac{D}{l}}{\frac{1}{2}\rho U_{\tau e^{iC}}} = \frac{\frac{\text{Drag force}}{\text{unit lenght}}}{\frac{\text{Dynamic force}}{\text{unit lenght}}} \tag{3}$$

where c is the airfoil chord length, l is the airfoil span, L is the lift force, and D is the drag force.

2.3. The SG6043 airfoil modified optimization. Figure 2a presents a comparison of the peak CL/CD concerning the t/c for the SG6043 airfoil across Reynolds numbers (Re) ranging from 10,000 to 500,000, based on preliminary design optimization results. As depicted in Fig. 2a, there exists a dome-shaped relationship between the thickness-to-camber ratio and the peak CL/CD at each Re. Generally, the CL/CD efficiency demonstrated an increase with higher Re values. The most optimal airfoil, delivering the highest lift-to-drag ratio, was consistently associated with specific t/c values across all Re studied. Consequently, the modified airfoil's maximum t/c varied within the range of 0.5 to 1.5. Deviating from this t/c range resulted in decreased peak CL/CD. The study focused on an ideal t/c falling between 0.50 and 1.50, serving as a basis for determining the thickness and camber of the newly designed airfoil.

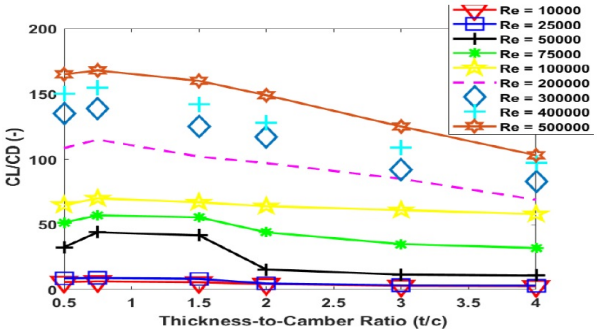

(A) The peak CL/CD at various t/c

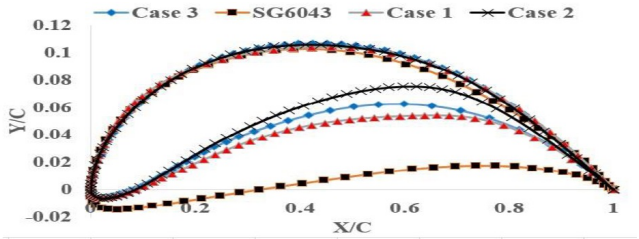

(B) The SG6043 and modified airfoils

FIGURE 2. Airfoil geometry variation for SG6043 airfoil optimization

The optimized specifications for Case 1 airfoil include a peak thickness of 7.05 located at 17.20 of the chord, along with a peak camber of 7.72 positioned at 49.80 of the chord. Case 2 airfoil, on the other hand, is optimized with a peak thickness of 6.52 situated at 15.30 of the chord and a peak camber of 8.79 located at 53.20 of the chord. Finally, Case 3 airfoil is designed to feature a peak thickness of 6.60

positioned at 15.30 of the chord and a peak camber of 8.30 at 50.30 of the chord, as visually depicted in Fig. 2b. In contrast, the SG6043 airfoil showcases a peak thickness of 10.02 at 32.10 of the chord and a peak camber of 5.50 situated at 49.70 of the chord. These parameters fall within the t/c range of 0.50 to 1.50, which guided the development of the three designated airfoils: Case 1, Case 2, and Case 3. Figure 2b illustrates a substantial contrast between the SG6043 airfoil and the newly modified Case airfoils, particularly in the geometric profiles of thickness and camber. Notably, the Case airfoils exhibit thinner profiles and greater camber compared to the SG6043 airfoil. As previously mentioned, the efficiency parameters of these newly designed airfoils and the SG6043 airfoil were evaluated across a Reynolds number (Re) range from 10,000 to 500,000

3. Results and discussions

3.1. Validation data. The findings obtained from QBLADE software were compared to the aerodynamic characteristics predicted by Burdett et al.'s experimental data [3] at a Re of 200,000 for the S823 airfoil, as depicted in Fig. 3a. The comparison in Fig. 3a demonstrates a reasonable agreement between the QBLADE software data and the experimental results by Burdett et al. [3]. Therefore, the investigation's results indicated a similar increasing trend.

In addition, a further validation case at Re of 200,000 utilizing the Eppler 387 airfoil was conducted to enhance confidence in the QBLADE software. The drag polar obtained by the SST Transitional model by Willems et al. [25], experimental data [20], and the present QBLADE software were compared in Fig. 3b. The QBLADE software, employing the SST Transitional Model, exhibited significant agreement with the experimental results across a wide range of AoA, as depicted in Fig. 3b. This reaffirms the suitability of utilizing this specific model for our objectives.

3.2. Comparison of CL, CD, drag buckets, and CL/CD of SG6043 and SG6043 modified airfoils. Figure 4a depicts the CL efficiency graph comparing the SG6043 airfoil to the modified airfoils at a Re of 10,000. This figure illustrates that the CL of the Case airfoils surpasses that of the SG6043 airfoil. Specifically, the Case 2 airfoil exhibited improved lift performance for AoAs greater than 4°, while the modified airfoils displayed similar lift efficiency trends above 4° AoA. Notably, the Case 2 airfoil achieved the highest maximum CL of 1.357, while the base airfoil had the lowest peak CL of 1.05. Additionally, Case 3 and Case 1 airfoils reached peak CL values of 1.315 and 1.310, respectively. Both the SG6043 and Case airfoils demonstrated a stall AoA of up to 20°, marking the largest stall AoA.

Figure 4b highlights the superior drag bucket performance of the Case airfoils compared to the SG6043 airfoil. All four airfoils exhibited gradual early lift increases without corresponding rises in drag. However, the SG6043 airfoil experienced a

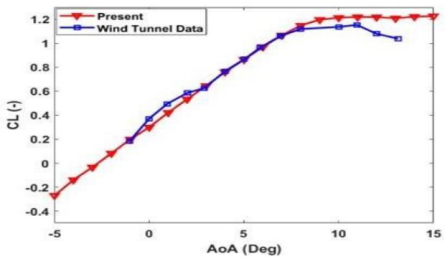

(A)

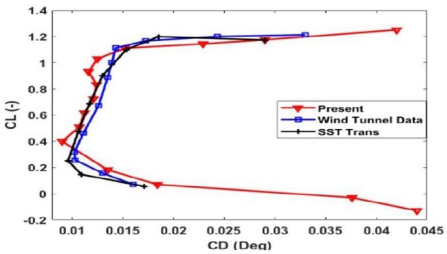

(B)

FIGURE 3. Comparison and validation (a) the current QBLADE software data with experiment data by Burdett et al. [3] (b) the current QBLADE software data with the SST Transitional model (Willems et al. [25]) and experimental data by Selig and Guglielmo [20]

significant increase in drag beyond a CL of 0.283. As the CL of the Case airfoils exceeded 0.65, their CD began to rise, initially maintaining a constant level. Notably, differences in performance among the modified airfoils primarily surfaced above a CD of 0.0734. Here, the Case 2 airfoil demonstrated the most favorable performance in the drag bucket, followed by the Case 3 and Case 1 airfoils.

Figure 4c shows the CL/CD performance of the original and Case airfoils at Re of 10000. According to Fig. 4c, the Case airfoils perform better in CL/CD investigates than the original SG6043 airfoil, particularly for AoA between 4° to 20°. The highest maximum CL/CD of 9.02 was recorded by Case 1 airfoil at an AoA of 4°, while the lowest peak value was obtained by SG6043 airfoil at an AoA of 5°, where it was 6.62. Moreover, the maximum CL/CD values for Cases 2 and 3 airfoils were 8.85 at an AoA of 4° and 8.43 at an AoA of 4°, respectively. At Re 25000, Fig. 5a displays the CL efficiency graphs for the SG6043 and Case airfoils. The graph indicates that the Case airfoils have a higher CL than the SG6043 airfoil. Up to an AoA of 8°, the lift performance trends for Case 2 and 3 airfoils were similar; however, beyond 8°, Case 2 showed improved lift performance. Notably, the maximum CL peaked at 1.428 for Case 2 and 1.12 for SG6043. Case 3 and Case 1 achieved peak CL values of 1.40 and 1.398, respectively. Fig. 5a illustrates that both SG6043 and Case airfoils reach a

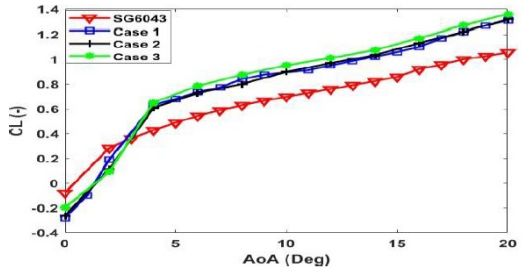

(A) The CL of SG6043 and Case airfoils

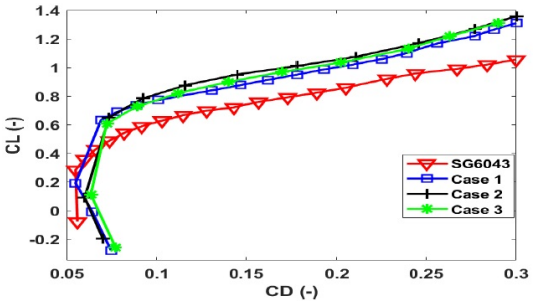

(B) Drag buckets for SG6043 and Case airfoils

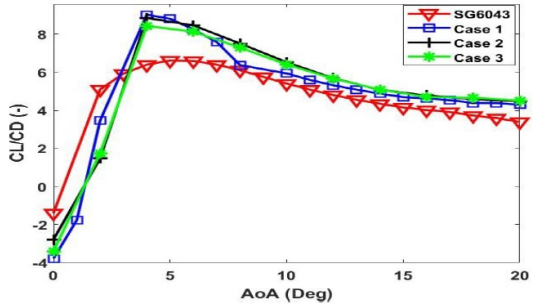

(C) The CL/CD performance of SG6043 and Case airfoils

FIGURE 4. Comparison of CL, drag buckets, and CL/CD of SG6043 and Case airfoils at Re of 10000

stall AoA of 20°, while Case 3 and Case 1 airfoils stall at the same angle. In Figure 5b, the drag bucket performance of the Case airfoils surpasses that of the SG6043 airfoil. Initially, all airfoils experience slow lift increases without corresponding rises in drag. However, the SG6043 airfoil's drag begins to rise beyond CL 0.32. In contrast, the Case airfoils show drag increments at a notably higher CL, around 0.46. Notably, the performance disparities among the Case airfoils primarily emerge

above CD 0.06, where the Case 2 airfoil excels in the drag bucket, followed by the Case 1 and 3 airfoils.

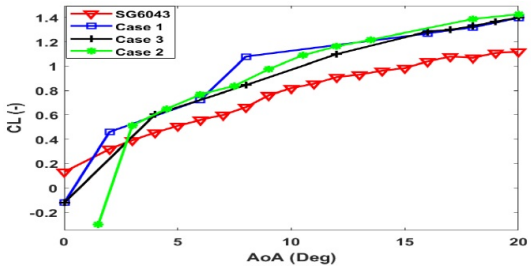

(A) The CL of SG6043 and Case airfoils

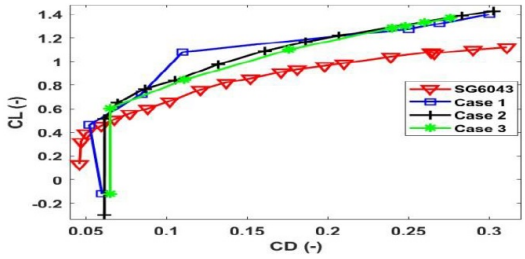

(B) Drag buckets for SG6043 and Case airfoils

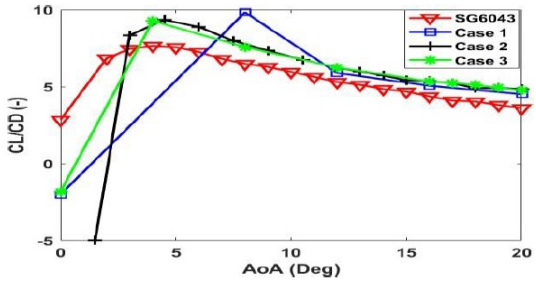

(C) The CL/CD performance of SG6043 and Case airfoils

FIGURE 5. Comparison of CL, drag buckets, and CL/CD of SG6043 and Case airfoils at Re of 25000

At Re 25000, Fig. 5c investigates the CL/CD efficiency of the SG6043 and Case airfoils. The analysis demonstrates the superior performance of the Case airfoils compared to the SG6043 airfoil in CL/CD assessments, particularly evident between AoAs of 3° to 20° for Case 2 and Case 3 airfoils, and from 8° to 20° for Case 1. Specifically, at a 4° AoA, Case 1 reached a maximum peak CL/CD of 10.3, while the SG6043 airfoil reported the lowest peak value of 7.66. Additionally, Cases 2 and 3 achieved peak CL/CD values of 9.36 at 5° AoA and 9.27 at 4° AoA, respectively. In

Figure 6a, the efficiency curves of the SG6043 and Case airfoils at Re 50000 reveal that the Case airfoils exhibit higher CL values compared to the SG6043 airfoil. While the lift efficiency trends of the Case airfoils were similar between AoAs of 2° to 8°, the Case 2 airfoil demonstrated notably superior lift performance beyond 2° AoA. Notably, the SG6043 airfoil had its lowest peak CL at 1.554, whereas the Case 2 airfoil achieved the highest peak CL at 1.847. Additionally, Case 1 and Case 3 airfoils reached peak CL values of 1.814 and 1.77, respectively. The maximum stall AoA observed was 12° for both SG6043 and Case 2 airfoils, while Cases 3 and 1 had a stall AoA of 11°. In Fig. 6b, the drag bucket efficiency of the Case airfoils outperformed that of the SG6043 airfoil. Initially, all airfoils experienced a gradual increase in lift accompanied by slow drag rises, but the SG6043 airfoil's drag escalated rapidly at CL 0.26. Conversely, the drag for the Case airfoils started to rise at a somewhat higher CL, approximately 0.40. Notably, above CD 0.062, the Case 2 airfoil excelled, followed by the Case 1 and 3 airfoils, showcasing performance differences among the Case airfoils in the drag bucket region.

At Re 50000, Fig. 6c compares the CL/CD performance between the SG6043 and Case airfoils. This analysis indicates that the Case airfoils outperform the SG6043 airfoil in CL/CD assessments, particularly evident across AoAs ranging from 3° to 14° for all Case airfoils. Specifically, Case 1 achieved the highest peak CL/CD of 44.60 at a 7° AoA, while the SG6043 airfoil displayed the lowest peak value of 38.56 at a 9° AoA. Additionally, Case 2 reached peak CL/CD values of 42.31 at a 9° AoA, and Case 3 reached 41.54 at a 9° AoA, respectively.

At Re 50000, Figure 7a compares the CL/CD performance between the SG6043 and Case airfoils. This comparison highlights the superior performance of the Case airfoils in CL/CD assessments, particularly evident across AoAs ranging from 3° to 14° for all Case airfoils. Notably, Case 1 achieved the highest peak CL/CD of 44.60 at a 7° AoA, while the SG6043 airfoil displayed the lowest peak value of 38.56 at a 9° AoA. Furthermore, Case 2 reached peak CL/CD values of 42.31 at a 9° AoA, and Case 3 reached 41.54 at a 9° AoA, respectively.

In Figure 7b, the drag bucket performance of the Case airfoils outshines that of the SG6043 airfoil. Initially, all four airfoils experienced gradual lift increases without corresponding rises in drag. However, the SG6043 airfoil's drag sharply escalated above CL 1.342. On the contrary, the drag on the Case airfoils didn't start increasing until reaching a higher CL around 1.36. Notably, performance distinctions among the Case airfoils predominantly emerged above CD 0.0284, where the Case 2 airfoil showcased the best performance in the drag bucket, followed by the Case 1 and 3 airfoils.

In Figure 7c, the CL/CD efficiency of the SG6043 and Case airfoils at Re 75000 is depicted. This comparison highlights the superior performance of the Case airfoils over the SG6043 airfoil in CL/CD assessments, notably noticeable for AoAs between

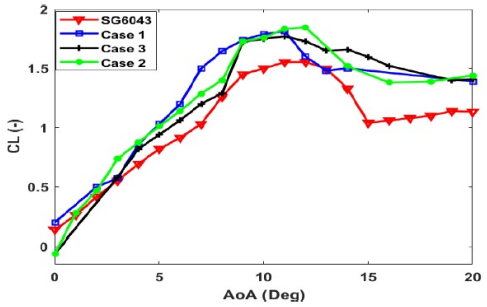

(A) The CL of SG6043 and Case airfoils

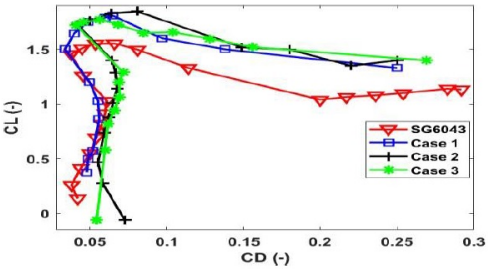

(B) Drag buckets for SG6043 and Case airfoils

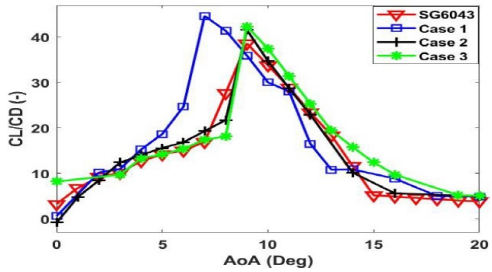

(C) The CL/CD performance of SG6043 and Case airfoils

FIGURE 6. Comparison of CL, drag buckets, and CL/CD of SG6043 and Case airfoils at Re of 50000

4° to 7° for Case 1, 3° to 8° for Case 2, and 8° to 10° for Case 3. The SG6043 airfoil showcased the lowest peak CL/CD of 50.94 at a 7° AoA, while the Case 3 airfoil reached the highest peak CL/CD of 57.42 at an 8° AoA. Additionally, the peak CL/CD values were 55.50 for the Case 2 airfoil at a 7° AoA and 55.28 for the Case 1 airfoil at a 7° AoA, respectively.

In Figure 8a, an analysis of the CL efficiency curves of the SG6043 and Case airfoils at Re 100000 demonstrates that the Case airfoils exhibit higher CL values

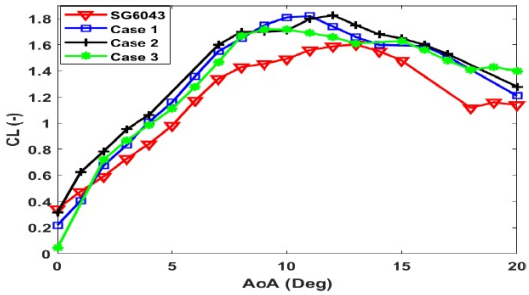

(A) The CL of SG6043 and Case airfoils

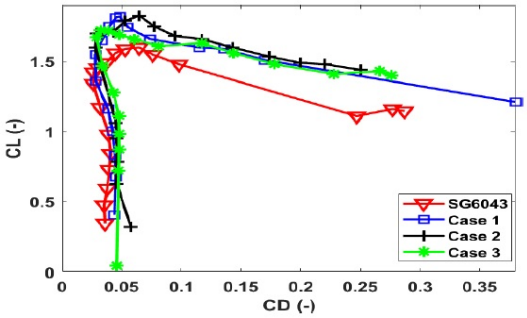

(B) Drag buckets for SG6043 and Case airfoils

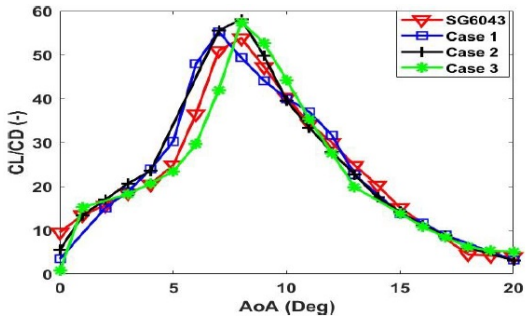

(C) The CL/CD performance of SG6043 and Case airfoils

FIGURE 7. Comparison of CL, drag buckets, and CL/CD of SG6043 and Case airfoils at Re of 75000

compared to the SG6043 airfoil. Although the lift performance trends of the Case airfoils were similar between AoAs of 1° to 8°, the Case 1 airfoil displayed increased lift efficiency beyond 2° AoA. Notably, the SG6043 airfoil had a peak CL of 1.604, while the Case 1 airfoil reached 1.79. Additionally, the peak CL values were 1.748 for Case 2 and 1.70 for Case 3 airfoils. The largest stall AoA observed was 12° for

the Case 2 airfoil, while Case 1 and 3 airfoils had respective stall AoA values of 10° and 9°.

In Figure 8b, the drag bucket performance of the Case airfoils surpasses that of the SG6043 airfoil. Initially, all four airfoils experienced gradual lift increases without corresponding rises in drag. However, the SG6043 airfoil's drag sharply escalated above CL 1.54. On the other hand, for the Case airfoils, drag didn't increase until reaching a CL of 1.45. Notably, performance distinctions among the Case airfoils primarily emerged above CD 0.0208, where the Case 1 airfoil demonstrated the best performance in the drag bucket, followed by the Case 2 and 3 airfoils.

The CL/CD efficiency of the SG6043 and Case airfoils at Re 100000 is presented in Fig. 8c. The analysis illustrates that the Case airfoils outperform the SG6043 airfoil in CL/CD tests, notably noticeable for AoAs between 5° to 6° for Case 1, 5° to 9° for Case 2, and 7° to 10° for Case 3. The SG6043 airfoil showcased the lowest peak value at 65.86 with a 7° AoA, while Case 2 attained the highest peak CL/CD of 73.08 at a 7° AoA. Additionally, the maximum CL/CD values were 70.33 for Case 3 at a 7° AoA and 69.48 for the Case 1 airfoil at a 6° AoA, respectively.

In Figure 9a, the CL efficiency graph of the SG6043 and Case airfoils at Re 200000 is displayed. The data illustrates that the Case airfoils exhibit higher CL values than the SG6043 airfoil. Notably, the Case 2 airfoil demonstrated enhanced lift performance for AoAs greater than 0°, despite the airfoils showing similar lift efficiency trends for AoAs above 0°. Moreover, the Case 2 airfoil reached the highest maximum CL at 1.743, while the SG6043 airfoil achieved the lowest peak CL at 1.595. Additionally, Case 1 and Case 3 airfoils attained peak CL values of 1.732 and 1.677, respectively. The Case 2 airfoil also displayed the largest stall AoA, reaching 12°, while Case 1 and Case 3 airfoils had stall AoA values of 11° and 10°, respectively. Furthermore, the stall efficiency of the Case 2 airfoil appeared to be the most gradual among the Case airfoils.

In Figure 9b, it's evident that the Case airfoils outperformed the SG6043 airfoil in terms of drag bucket performance. Initially, all four airfoils experienced gradual lift gains without corresponding increases in drag, but the SG6043 airfoil's drag sharply increased above CL 1.427. In contrast, the drag on the Case airfoils began to rise at a slightly higher CL, approximately 1.45. Notably, the Case 2 airfoil exhibited superior performance in the drag bucket, followed by the Case 1 and 3 airfoils. Noteworthy differences in performance among the Case airfoils primarily emerged above the CD of 0.0145.

In Figure 9c, the CL/CD efficiency of the SG6043 and Case airfoils at a Re of 200,000 is presented. The figure illustrates that in CL/CD analysis, the Case airfoils outperform the SG6043 airfoil, especially within specific Angle of Attack (AoA) ranges: 3° to 5° for Case 1, 4° to 7° for Case 2, and 4° to 7° for Case 3. The SG6043 airfoil showed the lowest peak value at an AoA of 5°, measuring 97.21, while

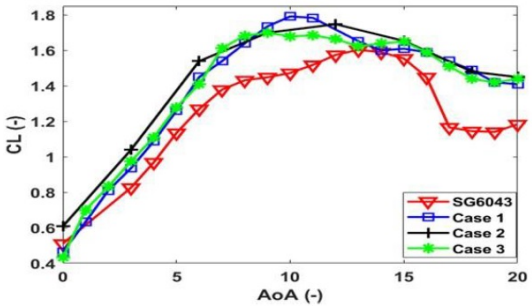

(A) The CL of SG6043 and Case airfoils

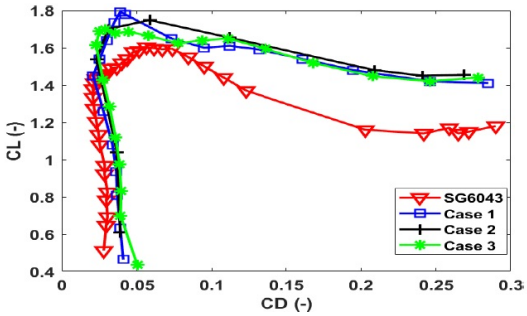

(B) Drag buckets for SG6043 and Case airfoils

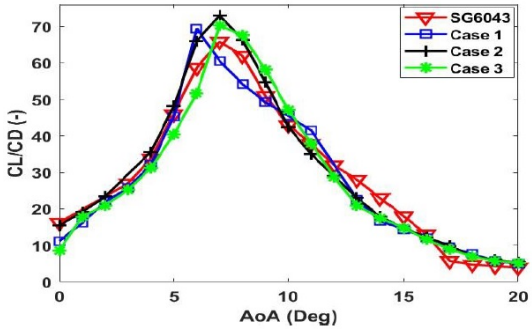

(C) The CL/CD performance of SG6043 and Case airfoil

FIGURE 8. Comparison of CL, drag buckets, and CL/CD of SG6043 and Case airfoils at Re of 100000

Case 2 had the highest peak CL/CD of 111.7 at an AoA of 5°. Moreover, Case 3 and Case 1 airfoils achieved peak CL/CD values of 109.58 and 108.47 respectively, at AoAs of 6° and 5°.

The graph in Fig. 10a illustrates the CL efficiency of the Case and SG6043 airfoils at Re of 300,000. The CL of the modified SG6043 airfoils surpasses that of

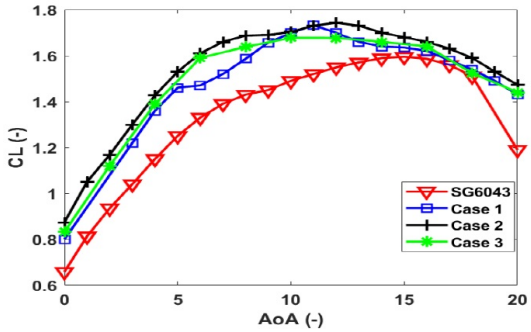

(A) The CL of SG6043 and Case airfoils

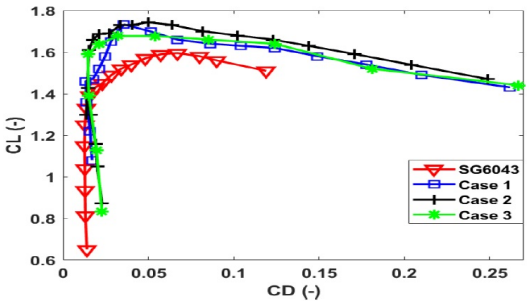

(B) Drag buckets for SG6043 and Case airfoils

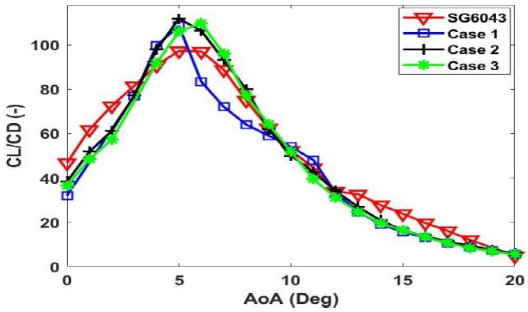

(C) The CL/CD performance of SG6043 and Case airfoils

FIGURE 9. Comparison of CL, drag buckets, and CL/CD of SG6043 and Case airfoils at Re of 200000

the original SG6043 airfoil. Although the Case airfoils exhibit similar lift efficiency trends for AoA above 0°, notably, Case 2 demonstrates enhanced lift performance for AoAs greater than 0°. Specifically, the SG6043 airfoil peaked at 1.634, while the highest CL for the Case 2 airfoil reached 1.756 at Re of 300,000. Additionally, the peak CL values for Case 1 and Case 3 airfoils were 1.72 and 1.696, respectively.

Among them, the Case 2 airfoil exhibited the largest stall AoA at 13°, while Case 1 and Case 3 airfoils stalled at 12°.

Figure 10b showcases how the Case airfoils outperformed the SG6043 airfoil in terms of drag bucket performance. Initial lift gains across the entire airfoils were gradual without corresponding increases in drag. However, the drag for the SG6043 airfoil started rising sharply beyond a CL of 1.36, while the Case airfoils experienced a drag increase at a slightly higher CL, around 1.46. Notably, the Case 2 airfoil exhibits superior performance within the drag bucket, followed by the Case 1 and Case 3 airfoils. Notable performance distinctions between the Case airfoils primarily manifest above a CD of 0.0105.

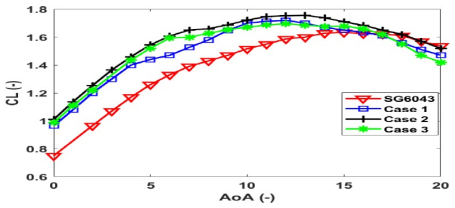

(A) The CL of SG6043 and Case airfoils

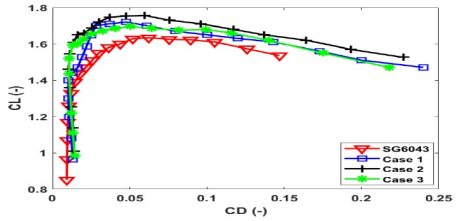

(B) Drag buckets for SG6043 and Case airfoils

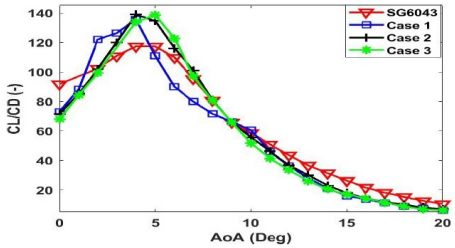

(C) The CL/CD performance of SG6043 and Case airfoils

FIGURE 10. Comparison of CL, drag buckets, and CL/CD of SG6043 and Case airfoils at Re of 300000

In Figure 10c, the CL/CD efficiency of the SG6043 and Case airfoils at a Re of 300,000 is depicted. The figure illustrates that in CL/CD analysis, the Case airfoils outperform the SG6043 airfoil, especially within specific Angle of Attack (AoA) ranges: 2° to 4° for Case 1, 3° to 7° for Case 2, and 3° to 7° for Case 3. The SG6043 airfoil exhibited the lowest peak value at an AoA of 4°, measuring 117.25, while Case 2 reached the highest peak CL/CD of 138.67 at an AoA of 4°. Additionally, the peak CL/CD values for Case 3 at an AoA of 5° and Case 1 at an AoA of 4° were 138.37 and 135.59 respectively.

In Figure 11a, the CL efficiency graph for the SG6043 and Case airfoils at a Re of 400,000 is depicted. The Case airfoils exhibit higher CL values compared to the SG6043 airfoil. Specifically, despite the Case airfoils showing similar lift trends up to an AoA of 0°, the Case 2 airfoil demonstrates superior lift performance for AoAs above 0°. The peak CL for the SG6043 airfoil was 1.697, whereas the highest CL among the Case airfoils was recorded by Case 2 at 1.77. Additionally, the peak CL values for Case 1 and Case 3 airfoils were 1.74 and 1.72 respectively. Notably, the stall AoA for Case 2 reached 13°, while Case 1 and Case 3 airfoils stalled at 12°.

Figure 11b illustrates how the Case airfoils outperform the SG6043 airfoil in terms of drag bucket performance. Initially, lift gains across the entire airfoils were gradual without corresponding increases in drag. However, the drag for the SG6043 airfoil began sharply rising beyond a CL of 1.37. In contrast, the drag on the Case airfoils increased at a slightly higher CL, approximately 1.467. Notably, the Case 2 airfoil exhibits superior performance within the drag bucket, followed by the Case 1 and Case 3 airfoils. Noticeable performance distinctions between the Case airfoils predominantly manifest above a CD of 0.0091.

In Figure 11c, the CL/CD efficiency of the SG6043 and Case airfoils is presented at a Re of 400,000. The figure indicates that in the CL/CD study, the Case airfoils outperform the SG6043 airfoil, particularly within Angle of Attack (AoA) ranges: 0° to 5° for Case 1, 2° to 6° for Case 2, and 2° to 6° for Case 3. The SG6043 airfoil showcased the lowest peak value, 132.54, at an AoA of 4°, while Case 2 reached the highest peak CL/CD of 160.80 at an AoA of 3°. Additionally, Case 3 at an AoA of 4° and Case 1 at an AoA of 4° recorded the highest CL/CD values, measuring 159.93 and 154.30, respectively.

In Figure 12a, the CL efficiency graph for the SG6043 and Case airfoils at a Re of 500,000 is depicted. The modified SG6043 airfoils exhibit higher CL values than the original SG6043 airfoil. Notably, while the other Case airfoils showed similar lift performance trends up to an AoA of 0°, the Case 2 airfoil displayed superior lift performance for AoAs above 0°. The peak CL for the SG6043 airfoil was 1.732, whereas the highest CL among the Case airfoils was achieved by Case 2 at 1.79. Additionally, the peak CL values for Case 1 and Case 3 airfoils were 1.75 and 1.735

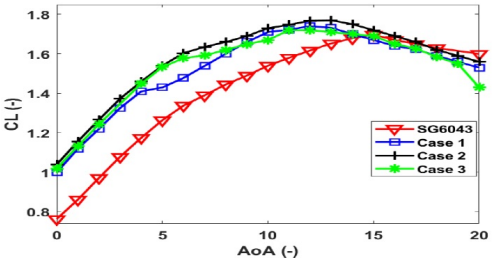

(A) The CL of SG6043 and Case airfoils

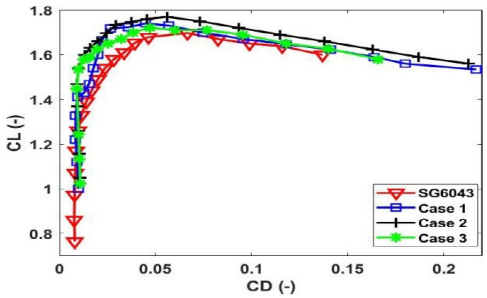

(B) Drag buckets for SG6043 and Case airfoils

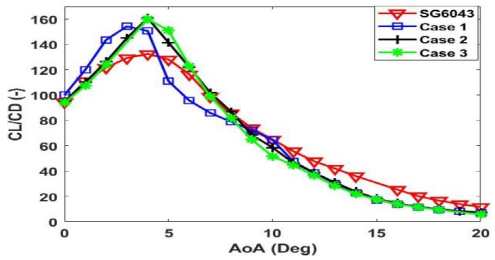

(C) The CL/CD performance of SG6043 and Case airfoils

FIGURE 11. Comparison of CL, drag buckets, and CL/CD of SG6043 and Case airfoils at Re of 400000

respectively. Noteworthy is the stall AoA, with Case 2 reaching the highest at 13°, while Case 1 and Case 3 airfoils stalled at 12°.

In Figure 12b, it's illustrated that the modified SG6043 airfoil surpassed the original SG6043 airfoil in terms of drag bucket performance. Initially, lift gains across the entire airfoils were gradual without corresponding increases in drag. However, the drag for the SG6043 airfoil started sharply rising beyond a CL of 1.38. In contrast, the drag on the Case airfoils increased at a slightly higher CL, approximately 1.53. Notably, the Case 2 airfoil demonstrates superior performance within the drag

bucket, followed by the Case 1 and Case 3 airfoils. Distinctions in performance between the Case airfoils predominantly manifest above a CD of 0.0096.

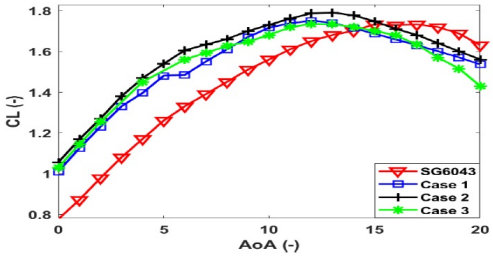

(A) The CL of SG6043 and Case airfoils

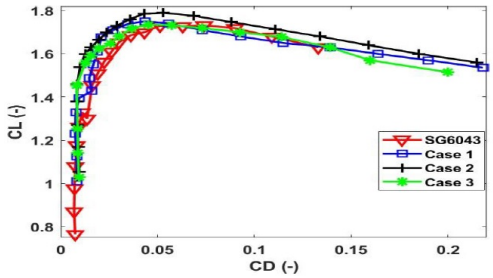

(B) Drag buckets for SG6043 and Case airfoils

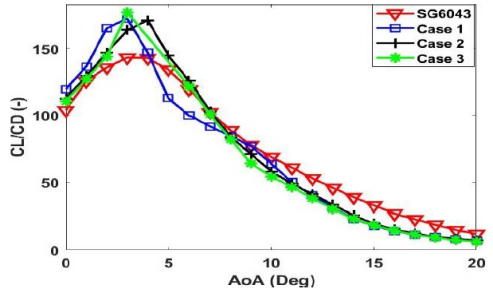

(C) The CL/CD performance of SG6043 and Case airfoils

FIGURE 12. Comparison of CL, drag buckets, and CL/CD of the Case and SG6043 airfoils at Re of 500000

Figure 12c illustrates the CL/CD efficiency of the SG6043 and Case airfoils at a Re of 500,000. The modified SG6043 airfoils outperform the original SG6043 airfoil, particularly within Angle of Attack (AoA) ranges: 1° to 4° for Case 1, 1° to 6° for Case 2, and 1° to 6° for Case 3, as indicated in Fig. 12c. At an AoA of 3°, the SG6043 airfoil recorded the lowest peak value of 143.33, whereas Case 3 achieved the

highest peak of 176.97 at the same AoA. Furthermore, the greatest CL/CD values were observed for Case 1 at an AoA of 3° and Case 2 at an AoA of 4°, measuring 172.43 and 171.08 respectively.

3.3. Summary of performance and technical analysis. Figures 13 and 14 present the lift, stall, and CL/CD summaries for the Case 1, 2, and 3 airfoils. In Fig. 13a, the Case 2 airfoil displayed the highest peak CL within the investigated Re range of 10,000 to 75,000, while the Case 1 airfoil exhibited the lowest peak CL among the modified airfoils within the Re range of 10,000 to 25,000. Additionally, at the Re range of 50,000 to 100,000, the Case 3 airfoil showcased the lowest peak CL, whereas the Case 1 airfoil demonstrated the highest peak CL at the Re of 100,000. Furthermore, within the investigated Re range of 200,000 to 500,000, the Case 2 airfoil had the highest peak CL, while the Case 3 airfoil recorded the lowest peak CL at the Re of 200,000 among the modified airfoils. Additionally, at the investigated Re range of 300,000 to 500,000, the Case 3 airfoil displayed the lowest peak CL.

As previously discussed, Fig. 13b indicates that the SG6043 airfoil consistently displayed the lowest peak CL across all investigated Re values from 10,000 to 500,000. Additionally, Fig. 13a shows that both the Case and SG6043 airfoils shared the same stall AoA at Re of 10,000 and 25,000. Furthermore, according to Fig. 13b, the Case 2 airfoil exhibited the highest stall AoA within the Re range of 50,000 to 500,000.

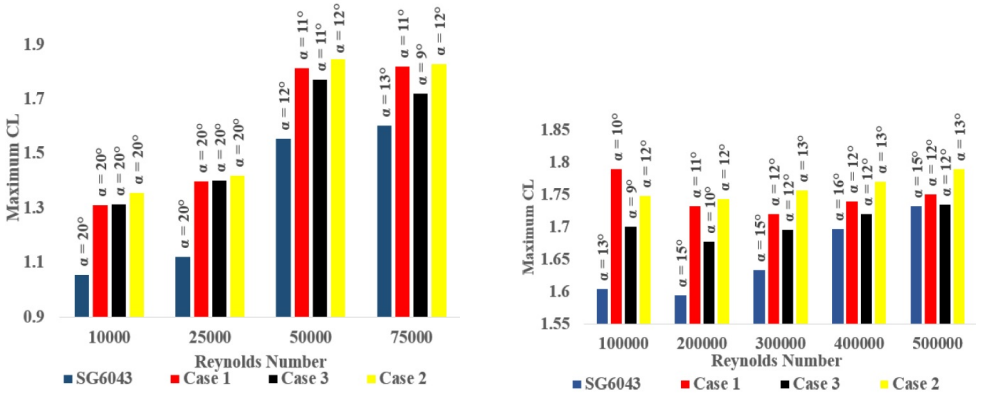

FIGURE 13. The lift and stall efficiency summary for modified airfoils

According to Fig. 14, as the Re increased from 10,000 to 500,000, the peak CL of all Case airfoils increased. Each airfoil exhibited its highest peak CL/CD at a Re of 500,000 and the lowest maximum CL/CD at a Re of 10,000. In Fig. 14a, at Re values below 500,000, the Case 1 airfoil outperformed the other Cases and

SG6043 airfoils, displaying the highest maximum CL/CD. At 75,000 Re, the Case 3 airfoil showcased the highest peak CL/CD, while the Case 2 airfoil held the highest peak CL/CD within the range of 100,000 to 400,000 Re. Additionally, at 500,000 Re, the Case 3 airfoil demonstrated the most exceptional peak CL/CD, reaching a maximum value of 176.97.

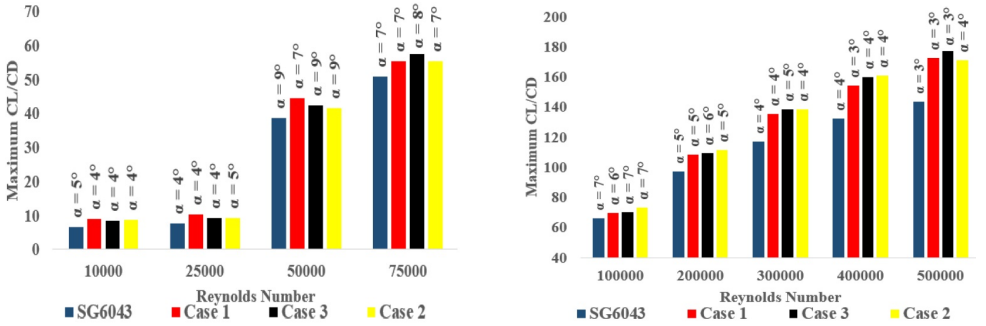

(A) (B)

FIGURE 14. The lift and stall efficiency summary for modified airfoils

The CL/CD data at Re values ranging from 10,000 to 500,000, as depicted in Fig. 15, is being compared with the results from other researchers [12, 13]. This comparison aims to evaluate the efficiency of the modified airfoils concerning airfoils designed in various studies for low Re and Small Wind Turbine (SWT) applications.

The comparison between the Case airfoils and the developed EYO-Series airfoils at Re 100,000 revealed that the Case airfoils exhibit a higher peak CL/CD than the EYO-Series counterparts. Notably, among the Case airfoils, Case 2 displayed superior efficiency compared to others. Similarly, at Re 200,000, the Case airfoils showcased greater peak CL/CD in comparison to both the EYO-Series and Case 2 proved to be more efficient than others in both series. This trend continued at Re 300,000, where the Case airfoils maintained higher peak CL/CD values than the EYO-Series, showcasing overall higher efficiency. Moreover, Case 2 remained the most efficient within the Case and EYO-Series airfoils. At Re 400,000, the data supported the trend, illustrating higher peak CL/CD for the Case airfoils against the EYO-Series, showcasing greater overall efficiency. Additionally, Case 2 exhibited the greatest CL/CD among all airfoils. Finally, at Re 500,000, the Case airfoils again displayed higher peak CL/CD values compared to the EYO-Series, with Case 3 exhibiting the highest peak CL/CD. These results underline the significance of factors like CL/CD, which significantly influence an airfoil's overall efficiency, where higher CL/CD ratios contribute to enhanced performance [12, 13].

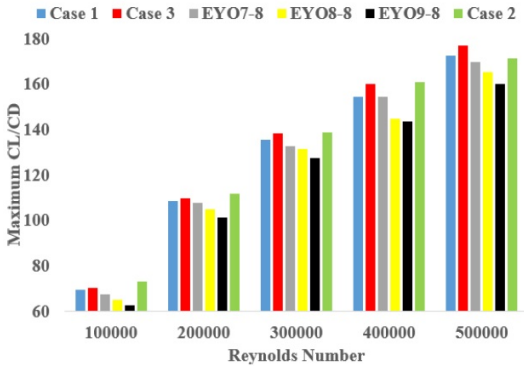

FIGURE 15. Comparison of Case airfoils with EYO-Series airfoils [12, 13] at Re of 100000 to 500000

4. Conclusions

In this study, the aerodynamic efficiency of the Case airfoils designed for Small Wind Turbine (SWT) application was assessed using QBLADE software. The investigations covered Re values up to 500,000, which is typical for SWT airfoils. The findings indicated a general trend of increased efficiency with rising Re values. The key conclusions drawn from the study were:

- The optimal thickness-to-chord ratio (t/c) fell within the range of 0.5 to 1.5 for the SG6043 airfoil, which displayed the highest lift-to-drag ratio within the Re range of 10,000 to 500,000.
- Case 3 airfoil achieved the highest CL/CD of 176.97 at Re of 500,000.
- The peak CL/CD values for Case 1 and 2 airfoils were 172.43 and 171.08, respectively.
- Case 2, 1, and 3 airfoils attained peak CL values of 1.847, 1.82, and 1.77, respectively.
- Throughout all investigated Re values, excluding Re of 100,000, Case 2 airfoil exhibited the highest CL compared to other modified and SG6043 airfoils.
- Drag bucket analyses indicated that Case airfoils enhanced lift efficiency, reaching peak lift while maintaining either constant or decreasing drag across the entire Re range.
- At $Re \leq 100,000$, the Case 1 airfoil displayed a higher maximum CL/CD than other modified and SG6043 airfoils.
- Within the Re range of 100,000 to 400,000, the Case 2 airfoil demonstrated the highest peak CL/CD.
- The Case airfoils showcased higher maximum CL/CD values compared to the EYO-Series airfoils within the Re range of 100,000 to 500,000.

The comparison between the present study and both experimental and Ansys Fluent data revealed that the data obtained from QBLADE software can reliably predict Ansys Fluent and wind tunnel results, showing a good match. Furthermore, the upcoming phase of the Solar Turbine Arta Energy (STAE) project will involve a comparative analysis between the modified airfoils at high Re and the SG6043 airfoil. Additionally, the research will extend to exploring other airfoils using different thickness-to-chord ratios (t/c) across various Re ranges. Finally, the plan includes the development of SG6043-modified airfoils for wind and tidal turbines, allowing for a direct comparison with turbines utilizing the standard SG6043 airfoil design.

List of Symbols

AoA	The angle of attack (Deg)
c	Chord length (m)
CL	Lift coefficient (-)
CD	Drag coefficient (-)
D	Drag force (N)
L	Lift force (N)
l	Airfoil span (m)
L/D	The lift-to-drag ratio (-)
Re	The Reynolds number (-)
U_{rel}	Air velocity (m/s)
X/C	Relative chord position (-)
Greek letters	
ρ	The density of the air (kg/m^3)
υ	Kinematic viscosity ($m^2 s^{-1}$)
μ	Dynamic viscosity ($Kg\ m^{-1} s^{-1}$)

References

[1] F. O. Akuffo, A. Brew-Hammond, J. Antonio, F. Forson, F. Edwin, A. Sunnu, A. Akwensivie, F. Agbeko, D. D. Ofori, and F. K. Appiah, *Solar and wind energy resource assessment (SWERA)*, Energy Commission, Ghana, 2003.

[2] C. . Bai, W. C. Wang, P. W. Chen, and W. T. Chong, *System integration of the horizontal-axis wind turbine: the design of turbine blades with an axial-flux permanent magnet generator*, Energies, **7**(11) (2014), 7773—7793.

[3] T. Burdett, J. Gregg, and K. Van Treuren, *An examination of the effect of Reynolds number on airfoil performance*, Energy Sustain., **54686** (2011), 2203–2213.

[4] F. Deng, C. Xue, and N. Qin, *Parameterizing airfoil shape using aerodynamic performance parameters*, AIAA Journal, **60**(7) (2022), 4399–4412.

[5] L. Hongpeng, W. Yu, Y. Rujing, X. Peng, and W. Qing, *Influence of the modification of asymmetric trailing-edge thickness on the aerodynamic performance of a wind turbine airfoil*, Renew. Energy, **147** (2020), 1623–1631.

[6] M. Islam, *Analysis of fixed-pitch straight-bladed VAWT with asymmetric airfoils*, Doctoral Thesis, University of Windsor, 2008.

[7] W. J. Koning, E. A. Romander, and W. Johnson, *Optimization of low Reynolds number airfoils for martian rotor applications using an evolutionary algorithm*, AIAA SciTech 2020 Forum, 2020, pp. 0084.

[8] D. S. Körpe and I. H. Güzelbey, *NACA four-digit airfoil series optimization: a comparison between genetic algorithm and sequential quadratic programming*, J. Mech. Sci. Technol., **37**(5) (2023), 1–8.

[9] A. Kumawat and S. Ghosh, *Numerical investigation of Hinged Flap vs. Morphed Trailing-edge at low Reynolds number*, AIAA SciTech 2023 Forum, 2023, pp. 2113.

[10] J. F. Manwell, J. G. Mcgowan, and A. L. Rogers, *Wind energy explained: theory, design and application*, Second Edition, John Wiley & Sons Ltd., 2009.

[11] S. Martel, M. Bashir, R. M. Botez, and T. Wong, *A Pareto multi-objective optimization of a camber morphing airfoil using non-dominated sorting genetic algorithm*, AIAA SciTech 2023 Forum, 2023, pp. 1583.

[12] E. Y. Osei, R. Opoku, A. K. Sunnu, and M. S. Adaramola, *Development of high performance airfoils for application in small wind turbine power generation*, J. Energy, **2020** (2020), 1–9.

[13] E. Y. Osei, R. Opoku, A. K. Sunnu, M. S. Adaramola, and E. A. Kyeremeh, *Aerodynamic performance characteristics of EYO-Series low Reynolds number airfoils for small wind turbine applications*, Alexandria Eng. J., **61** (2022), 12301–12310.

[14] X. Pang, H. Wang, and J. Chen, *Intelligence algorithm for optimization design of the low wind speed airfoil for wind turbine*, Cluster Comput., **22** (2019), 8119–8129.

[15] N. N. H. Quan and P. Van Lam, *Wind turbine blade design optimization using OpenFOAM and DAKOTA software*, Transport. Res. Proc. **56** (2021), 71–78.

[16] V. Raul and L. Leifsson, S*urrogate-based aerodynamic shape optimization for delaying airfoil dynamic stall using Kriging regression and infill criteria*, Aerospace Sci. Technol., **111** (2021), p. 106555.

[17] H. Seifi, S. Kouravand, M. S. Davary, and S. Mohammadzadeh, *Numerical and experimental study of the effect of increasing aspect ratio of self-starting force to vertical axis wind turbine*, J. Renew. New Energy, **10**(1) (2023), 1–14.

[18] H. Seifi, S. Kouravand, and M. Seifi Davary, *Numerical and experimental study of NACA airfoil in low Reynolds numbers for use of Darriues vertical axis micro-wind turbine*, J. Renew. New Energy, **10**(2) (2023), 149–163.

[19] H. Seifi Davari, S. Kouravand, M. Seify Davari, and Z. Kamalnejad, *Numerical investigation and aerodynamic simulation of Darrieus H-rotor wind turbine at low Reynolds numbers*, Energy Sources, Part A: Recov. Util. Environ. Effects, **45**(3) (2023), 6813–6833.

[20] M. S. Selig and J. J. Guglielmo, *High-lift low Reynolds number airfoil design*, J. Aircraft, **34**(1) (1997), 72-79.

[21] P. Sharma, B. Gupta, M. Pandey, A. K. Sharma, and R. N. Mishra, *Recent advancements in optimization methods for wind turbine airfoil design: A review*, Materials Today: Proc., **47** (2021), 6556–6563.

[22] Q. Song and W. David Lubitz, *Design and testing of a new small wind turbine blade*, J. Solar Energy Engin., **136**(3) (2014), 034502.

[23] H. E. Tanürün, *Improvement of vertical axis wind turbine performance by using the otimized adaptive flap by the Taguchi method*, Energy Sources, Part A: Recov. Util. Environ. Effects, **46**(1) (2024), 71–90.

[24] S. N. Uddin, M. R. Haque, M. M. Haque, M. F. Alam, and A. Hamja, *Numerical investigation of the enhancement of the aerodynamic performance for newly modified blended airfoils utilizing S809, S829, and NACA 2412 baseline shapes*, Arab. J. Sci. Eng., **49** (2024), 2233—2248.

[25] J. Willems, W. Engblom, and J. Wurts, *Verification, validation, and application of shear stress transport transitional model to a R/C aircraft*, AIAA Aerospace Sciences Meeting, 2018, pp. 2059.

Department of Mechanical and Marine Engineering, Chabahar Maritime University, Chabahar, Iran
Email address: hseifidavary@gmail.com

School of Engineering, RMIT University, Melbourne, VIC 3000, Australia
Email address: harun.chowdhury@abscube.com.au

Faculty of Engineering and Technology, Islamic Azad University, Germi, Iran
Email address: mohsenseify10@gmail.com

Department of Mathematics, Ardabil Branch, Islamic Azad University, Ardabil, Iran
Email address: hasanhosseinzadehmath@gmail.com,

Received : *December* 2023
Accepted : *February* 2024